Supporting Information

The Intrinsic Stability of Metal Ion Complexes with Nanoparticulate Fulvic Acids

Raewyn M. Town[1,4*], Jérôme F. L. Duval[2,3], and Herman P. van Leeuwen[4]

[1] Systemic Physiological and Ecotoxicological Research (SPHERE), Department of Biology, University of Antwerp, Groenenborgerlaan 171, 2020 Antwerp, Belgium. Email: raewyn.town@uantwerpen.be
[2] CNRS, Laboratoire Interdisciplinaire des Environnements Continenteaux (LIEC), UMR 7360, Vandoeuvre-lès-Nancy, F-54501 Nancy, France
[3] Université de Lorraine, LIEC, UMR 7360, Vandoeuvre-lès-Nancy, F-54501 Nancy, France
[4] Physical Chemistry and Soft Matter, Wageningen University & Research, Stippeneng 4, 6708 WE Wageningen, The Netherlands

The Supporting Information comprises 16 pages, and includes the derivation of eq 2 in the main text, Figure S1 showing the relative magnitude of counterion accumulation in the extraparticulate zone as compared to that within the FA body, explanation of the procedures used to obtain the water content and charge density of FA, and the $\overline{K}_{\mathrm{int}}$ values, Tables S1-S6 showing the sensitivity analysis for the computed $\overline{f}_{\mathrm{B}}^{(\mathrm{eq})}$ and $\overline{f}_{\mathrm{B}}^{(\mathrm{s})}$ values, Figures S2-S5 showing the sensitivity analysis for the $\overline{K}_{\mathrm{int}}$ values, Figure S6 showing the SSCP waves for CuHA, and the list of cited references.

Derivation of eq 2

The Poisson Boltzmann equation governing the distribution of the electrostatic potential $\psi(r)$ inside a charged soft NP with radius r_{p} and homogeneous charge density ρ_{o} in an aqueous medium containing *N* ions of valency z_i and bulk concentration c_i^{∞} is given by:

$$\nabla^2\psi(r) = -\frac{1}{\varepsilon_{\mathrm{o}}\varepsilon_{\mathrm{r}}}\left[\rho_{\mathrm{o}} + \sum_{i=1}^{N} F z_i c_i^{\infty} \exp\left(-z_i F\psi(r)/RT\right)\right] \tag{S1}$$

where r is the radial coordinate, and $r = 0$ being the soft particle center, $\nabla^2 = \mathrm{d}^2/\mathrm{d}r^2 + (2/r)\mathrm{d}/\mathrm{d}r$ is the Laplacian operator in spherical geometry, *F* is the Faraday number, *R* the gas constant, *T* the temperature and $\varepsilon_{\mathrm{o}}\varepsilon_{\mathrm{r}}$ the dielectric permittivity of the aqueous medium taken as identical to that in the NP body.[1,2] Application of eq S1 to a 2-1 electrolyte, *e.g.* $Ca(NO_3)_2$, leads to:

$$\frac{\mathrm{d}^2 y(r)}{\mathrm{d}r^2} + \frac{2}{r}\frac{\mathrm{d}y(r)}{\mathrm{d}r} = -\kappa^2\left\{\frac{\rho_{\mathrm{o}}}{2FI} + \frac{1}{3}\left[\exp\left(-2y(r)\right) - \exp\left(y(r)\right)\right]\right\} \tag{S2}$$

where we introduced the dimensionless electrostatic potential $y(r) = F\psi(r)/RT$, the solution ionic strength I and the extraparticulate electric double layer thickness $\kappa^{-1} = \left(\frac{2IF^2}{\varepsilon_o \varepsilon_r RT} \right)^{-1/2}$. In order to derive the typical decay length of the potential distribution from $r = 0$ to $r < r_p$, we adopt a strategy inspired by the work of Ohshima and applicable to the 1-1 electrolyte situation.[3] In detail, we write the potential $y(r)$ in the form $y(r) \approx y(r=0) + \Delta y(r)$. Substitution into eq S2 then yields:

$$\frac{d^2\Delta y(r)}{dr^2} + \frac{2}{r}\frac{d\Delta y(r)}{dr} = -\kappa^2 \left\{ \frac{\rho_o}{2FI} + \frac{1}{3}\left[\exp(-2y_{center}) \exp(-2\Delta y(r)) - \exp(y_{center}) \exp(\Delta y(r)) \right] \right\} \quad \text{(S3)}$$

where $y_{center} = y(r=0)$. After some algebra, the linearization of the right side of eq S3 with respect to $\Delta y(r)$ leads to:

$$\frac{d^2\Delta y(r)}{dr^2} + \frac{2}{r}\frac{d\Delta y(r)}{dr} = \kappa_p^2 \left\{ \Delta y(r) + \frac{\exp(-2y^D) - \exp(y^D) - \exp(-2y_{center}) + \exp(y_{center})}{2\exp(-2y_{center}) + \exp(y_{center})} \right\} \quad \text{(S4)}$$

where the dimensionless Donnan potential y^D – achieved in the NP body provided that the condition $\kappa r_p >> 1$ is satisfied – is defined by the transcendental equation:[4]

$$-\frac{3}{2}\frac{\rho_o}{FI} = \exp(-2y^D) - \exp(y^D) \quad \text{(S5)}$$

which is simply obtained from eq S2 taken in the extreme where the intraparticulate electric field is zero (*i.e.* $\nabla^2 y(r) = 0$). The quantity κ_p^{-1} involved in eq S4 has length dimension and is defined by the expression:

$$\kappa_p = \frac{\kappa}{\sqrt{3}}\left[2\exp(-2y_{center}) + \exp(y_{center}) \right]^{1/2} \quad \text{(S6)}$$

Adopting the boundary condition $dy/dr|_{r=0} = 0$ (symmetry argument) and $y(r=0) = y_{center}$, the solution of eq S4 may be written in the form:[3]

$$y(r) = y_{center} - F(y_{center}, y^D)\left\{ 1 - \frac{\sinh(\kappa_p r)}{\kappa_p r} \right\} \quad \text{(S7)}$$

with $F(y_{center}, y^D) = \frac{\exp(-2y^D) - \exp(y^D) - \exp(-2y_{center}) + \exp(y_{center})}{2\exp(-2y_{center}) + \exp(y_{center})}$. Equation S7 highlights that the characteristic decay length of the electrostatic potential within the soft NP particle identifies with $1/\kappa_p$, which corresponds to the result given in the main text.

Counterion Accumulation in the Extraparticulate Zone

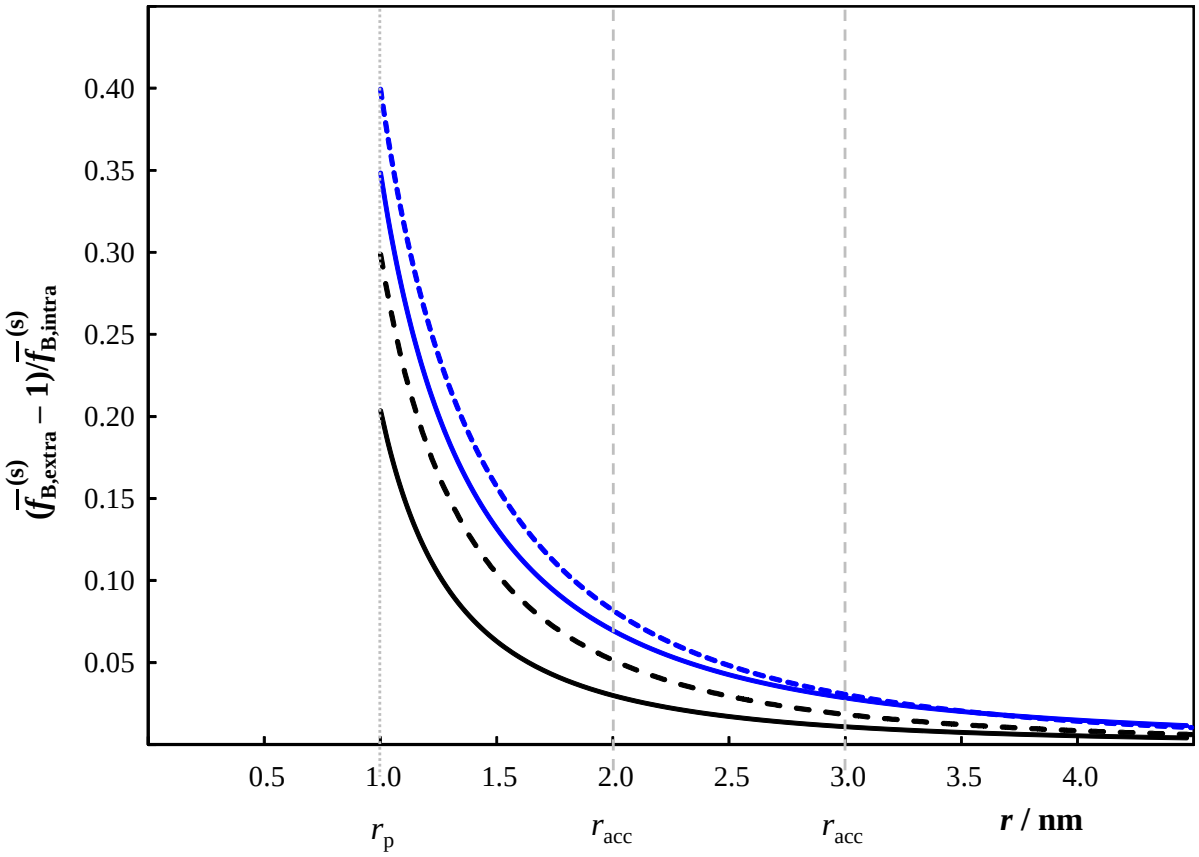

Figure S1. Relative magnitude of structural charge-derived 2+ counterion accumulation in the extraparticulate zone ($\overline{f}^{(s)}_{B,extra}\left(r > r_p\right)$) as compared to that within the particle body ($\overline{f}^{(s)}_{B,intra}$) for a particle of radius, r_p, of 1 nm and charge density of -2,000 mol e m^{-3} in various bulk electrolyte media. The curves correspond to 1-1 electrolyte at I = 10 mM (black solid curve) and 100 mM (black dashed curve), and 2-1 electrolyte at I = 10 mM (blue solid curve) and 100 mM (blue dashed curve). On the x-axis, r = 0 denotes the center of the soft particle body; r_p = 1 is the radius of the particle nm; and r_{acc} at 2 nm and 3 nm indicates the radius of the counterion accumulation volumes considered for interpreting data on electrostatic binding of metal by FA (see main text for details).

Water Content of Suwannee River Fulvic Acid (SRFA)

The density of the dry material = molar mass/molar volume. The density of SRFA = 1500 kg m^{-3},[5] and the reported molar mass is in the range *ca*. 550 – 1000 g mol^{-1}.[5-8] These values yield a molar volume in the range $3.7x10^{-4}$ to $6.7x10^{-4}$ m^3 mol^{-1} and thus a volume of $6.09x10^{-28}$ to $1.11x10^{-27}$ m^3 per individual FA entity. The hydrated particle radius of an FA entity is *ca.* 1 nm,[9] which corresponds to a hydrated particle volume of $4.19x10^{-27}$ m^3. Comparison of the hydrated volume with that calculated for the dry material yields a water content of *ca.* 74 to 85%.

Charge Density of SRFA

The charge density of SRFA at pH 6 is -10 meq gC^{-1},[10] which, for the 52% carbon content (IHSS data sheet), corresponds to -5.2 meq gFA^{-1}. The effective charge density within an FA entity will depend on the water content. From the density of SRFA,[5] the volume of 1 g of dry material follows as 1 g / $1.5x10^6$ g m^{-3} = $6.67x10^{-7}$ m^3. We consider the effective charge density to be homogeneously distributed within the hydrated particle body. Thus, if SRFA has a water content of 74%, the volume of 1 g of hydrated FA = $6.67x10^{-7}$ m^3/0.26 = $2.565x10^{-6}$ m^{-3}, and the charge density follows as $5.2x10^{-3}$ mol *e* / $2.565x10^{-6}$ m^{-3} ≈ -2000 mol *e* m^{-3}. Analogously, an 80% water content corresponds to a charge density of -1562 mol *e* m^{-3}, and an 85% water content corresponds to a charge density of -1170 mol *e* m^{-3}.

Computation of $\overline{K}_{\mathrm{int}}$ Values

The expression for the intrinsic stability constant $\overline{K}_{\mathrm{int}}$ is given as eq 6 in the main text, and repeated here for convenience:

$$\overline{K}_{\mathrm{int}} = \frac{c_{\mathrm{MS}}}{c_{\mathrm{S}} c_{\mathrm{M}}} \qquad \text{(S8)}$$

where c_{MS}, c_{M} and c_{S} are the *local* average concentrations of inner-sphere complexes, free metal ion and reactive sites in the particle body, respectively. In the present case, the total intraparticulate concentration of reactive sites, $c_{\mathrm{S,t}}$, corresponds to the concentration of charged sites (see preceding section) and $c_{\mathrm{S}} = c_{\mathrm{S,t}} - c_{\mathrm{MS}}$, c_{M} is obtained from $\overline{f}_{\mathrm{B}}\, c_{\mathrm{M}}^{*}$, where c_{M}^{*} is the concentration of the free metal ion in the bulk solution, and c_{MS} is obtained from the difference between the total and free metal ion concentration in the bulk solution, together with the aqueous particle volume fraction in the dispersion, and minus c_{M}. The particle-associated M is excluded from the volume occupied by the FA molecular backbone; evidently the accessible volume depends on the water content of the particles.

Sensitivity Analysis

A sensitivity analysis was performed on the computed $\overline{f}_{\mathrm{B}}^{(\mathrm{eq})}$ and $\overline{f}_{\mathrm{B}}^{(\mathrm{s})}$ values to assess the effect of the range of r_{p} reported for Suwannee River FA, i.e. 0.8 to 1.5 nm (corresponding to extremes of the Gaussian distribution of particle sizes),[9] the range of molar masses (550 – 1000 g mol^{-1}),[5-8] and the consequent charge densities and water contents (see above). For reasons detailed in the main text, $\overline{f}_{\mathrm{B}}^{(\mathrm{eq})}$ is more physicochemically sound than $\overline{f}_{\mathrm{B}}^{(\mathrm{s})}$ in the context of prediction of $\overline{K}_{\mathrm{int}}$ values. The agreement between the modelled ($\overline{f}_{\mathrm{B}}^{(\mathrm{eq})}$) and experimentally derived $\overline{K}_{\mathrm{int}}$ values is shown in companion figures, and the root mean squared error (RMSE) value for each case is given in the respective Figure captions ($\mathrm{RMSE} = \sqrt{\frac{1}{n}\sum_{n}[\log(\overline{K}_{\mathrm{int}})_{\mathrm{theory}} - \log(\overline{K}_{\mathrm{int}})_{\mathrm{experiment}}]^2}$, where the summation is over the number, *n*, of θ_{M} values at which $\overline{K}_{\mathrm{int}}$ was determined for the combined Cd and Cu datasets; see main text). Table 1 and Figure

3 in the main text show the outcomes for r_p = 1 nm, charge density = -2000 mol *e* m^{-3}, and water content = 74%. For these conditions, Figure S2 shows the experimental and modelled $\overline{K}_{int}$ data for CdFA and CuFA (same data as in Figure 3 of the main text), including the effect of the upper and lower limits of the experimental $\overline{f}_B$ values (given in Table 1, main text).

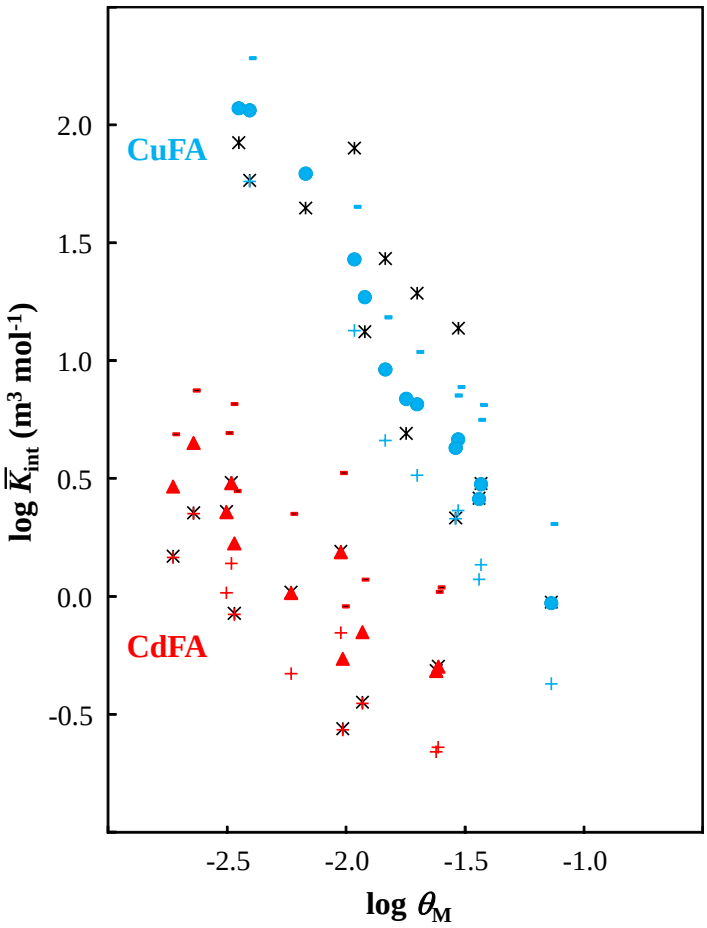

Figure S2. Comparison of the intrinsic stability constants, $\overline{K}_{int}$, determined for Cd(II) and Cu(II) complexes with fulvic acid (FA) as a function of the degree of occupation of reactive sites by inner-sphere complexes, i.e. the true θ_M (eq 7, main text). The relevant FA parameters are r_p = 1 nm, charge density = -2000 mol *e* m^{-3} and water content = 74%. The solid coloured points for CdFA (red triangles) and CuFA (blue dots) are obtained using the experimentally derived $\overline{f}_B$ values (Table 1, main text). The "+ "and "-" symbols correspond respectively to the upper and lower limits of the experimentally derived $\overline{f}_B$ values. The black asterisks are the values obtained using the modelled $\overline{f}_B^{(eq)}$ values (Table 1, main text, values not in parentheses). The RMSE between the modelled and experimental $\overline{K}_{int}$ values = 0.257.

The following Tables and Figures follow the same format as Table 1 in the main text and Figure S2. We note that changes in the charge density and water content also affect the experimentally derived $\overline{K}_{int}$ values: whilst the experimentally derived $\overline{f}_B$ is not changed, the intraparticulate reactive site density equates to the charge density and the water content affects the aqueous particle volume fraction which is used to obtain the intraparticulate concentration of inner-sphere complexes.

Table S1. Comparison of Computed and Experimentally-Derived Magnitudes of the Electrostatic Boltzmann Partitioning Coefficient, $\overline{f}_B$, for Divalent Cations for the case of r_p = 1 nm, charge density = -1562 mol *e* m^{-3}, water content = 80%. Values in parentheses correspond to different spatial zones of counterion accumulation. Experimental data correspond to Cd(II) and Cu(II) binding by FA.

Electrolyte and ionic strength	**Theoretical**		**Experimental**
	equilibrated charge, $\overline{f}_B^{(eq)}$	structural charge, $\overline{f}_B^{(s)}$	Figure 3[d]
KNO_3, I = 10 mM	19.88 [b] (5.50 [a])	10.52 [a] (29.45 [b])	26 (12-57)
KNO_3, I = 100 mM	0.57 [b] (NA [a])	2.15 [a] (4.45 [b])	5 (3-10)
$Ca(NO_3)_2$, I = 10 mM	7.46 [n_{Ca}=1.69] [a]	4.80 [a] (11.44 [b])	5 (3-10)
	(28.23 [n_{Ca}=1.90] [b])		
	(4.14 [n_{Ca}=1.49] [c])		
$Ca(NO_3)_2$, I = 100 mM	0.56 [n_{Ca}=0.38] [b] (NA [a])	1.63 [a] (2.80 [b])	1[e]

[a] integral from r = 0 to $r = r_p + 2$ nm, *i.e.* $\overline{f}_B^{(eq)}\left(r = r_{acc} = 3 \text{ nm}\right)$ or $\overline{f}_B^{(s)}\left(r = r_{acc} = 3 \text{ nm}\right)$

[b] integral from r = 0 to $r = r_p + 1$ nm, *i.e.* $\overline{f}_B^{(eq)}\left(r = r_{acc} = 2 \text{ nm}\right)$ or $\overline{f}_B^{(s)}\left(r = r_{acc} = 2 \text{ nm}\right)$

[c] integral from r = 0 to $r = r_p + 2.5$ nm, *i.e.* $\overline{f}_B^{(eq)}\left(r = r_{acc} = 3.5 \text{ nm}\right)$

[d] experimental $\overline{f}_B$ values are obtained from the difference between the dashed lines shown in Figure 3 in the main text. The range of values in parentheses is obtained from the standard errors on the regression lines (see Figure 2 caption in main text).

[e] reference electrolyte with *a priori* $\overline{f}_B$ value of unity

n_{Ca} is the average number of Ca^{2+} per FA

NA: not applicable, because a 2 nm extension of the condensation volume from the FA surface significantly exceeds the 0.96 nm extraparticulate Debye length operational in 100 mM solution ionic strength

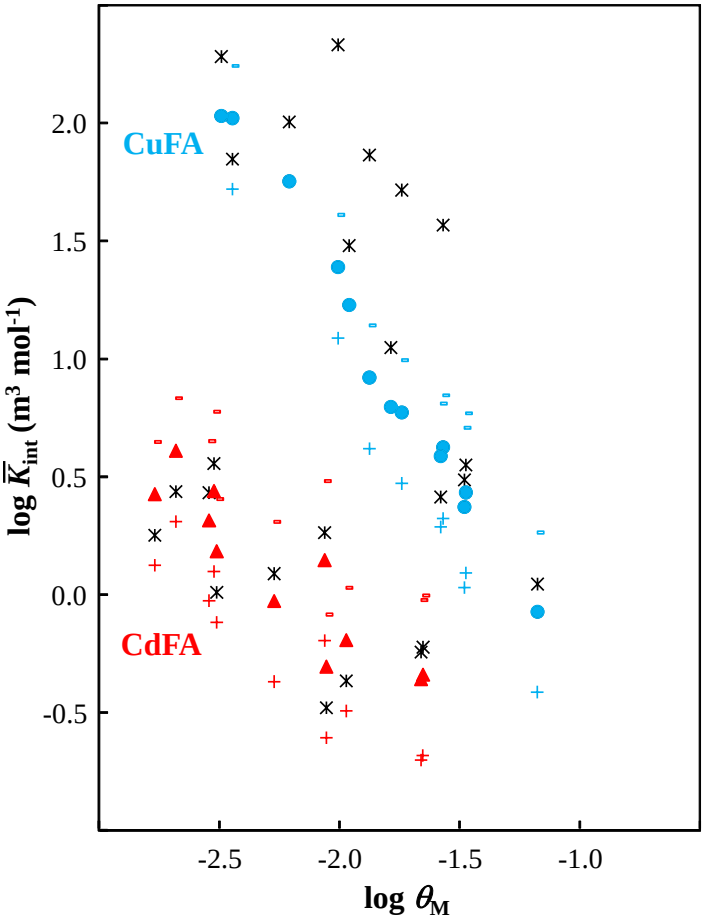

Figure S3. Comparison of the intrinsic stability constants, $\overline{K}_{int}$, determined for Cd(II) and Cu(II) complexes with fulvic acid (FA) as a function of the degree of occupation of reactive sites by inner-sphere complexes, i.e. the true θ_M (eq 7, main text). The relevant FA parameters are r_p = 1 nm, charge density = -1562 mol *e* m^{-3} and water content = 80%. The solid coloured points for CdFA (red triangles) and CuFA (blue dots) are obtained using the experimentally derived $\overline{f}_B$ values (Table 1, main text). The "+ "and "-" symbols correspond respectively to the upper and lower limits of the experimentally derived $\overline{f}_B$ values. The black asterisks are the values obtained using the modelled $\overline{f}_B^{(eq)}$ values (Table S1, values not in parentheses). The RMSE between the modelled and experimental $\overline{K}_{int}$ values = 0.416.

Table S2. Comparison of Computed and Experimentally-Derived Magnitudes of the Electrostatic Boltzmann Partitioning Coefficient, $\overline{f}_B$, for Divalent Cations for the case of r_p = 1 nm, charge density = -1170 mol *e* m^{-3}, water content = 85%. Values in parentheses correspond to different spatial zones of counterion accumulation. Experimental data correspond to Cd(II) and Cu(II) binding by FA.

Electrolyte and ionic strength	**Theoretical**		**Experimental**
	equilibrated charge, $\overline{f}_B^{(eq)}$	structural charge, $\overline{f}_B^{(s)}$	Figure 3[d]
KNO_3, I = 10 mM	14.60 [b] (3.77 [a])	4.75 [a] (11.16 [b])	26 (12-57)
KNO_3, I = 100 mM	NA [b] (NA [a])	1.66 [a] (2.89 [b])	5 (3-10)
$Ca(NO_3)_2$, I = 10 mM	5.28 [n_{Ca}=1.20] [a] (20.87 [n_{Ca}=1.41] [b]) (2.76 [n_{Ca}=1.00] [c])	3.35 [a] (7.06 [b])	5 (3-10)
$Ca(NO_3)_2$, I = 100 mM	NA [b] (NA [a])	1.45 [a] (2.24 [b])	1[e]

[a] integral from r = 0 to $r = r_p + 2$ nm, *i.e.* $\overline{f}_B^{(eq)}\left(r = r_{acc} = 3\text{ nm}\right)$ or $\overline{f}_B^{(s)}\left(r = r_{acc} = 3\text{ nm}\right)$

[b] integral from r = 0 to $r = r_p + 1$ nm, *i.e.* $\overline{f}_B^{(eq)}\left(r = r_{acc} = 2\text{ nm}\right)$ or $\overline{f}_B^{(s)}\left(r = r_{acc} = 2\text{ nm}\right)$

[c] integral from r = 0 to $r = r_p + 2.5$ nm, *i.e.* $\overline{f}_B^{(eq)}\left(r = r_{acc} = 3.5\text{ nm}\right)$

[d] experimental $\overline{f}_B$ values are obtained from the difference between the dashed lines shown in Figure 3 in the main text. The range of values in parentheses is obtained from the standard errors on the regression lines (see Figure 2 caption in main text)

[e] reference electrolyte with *a priori* $\overline{f}_B$ value of unity

n_{Ca} is the average number of Ca^{2+} per FA

NA[a]: not applicable, because a 2 nm extension of the condensation volume from the FA surface significantly exceeds the 0.96 nm extraparticulate Debye length operational in 100 mM solution ionic strength

NA[b]: not applicable. Indeed, decreasing the charge density (in absolute value) comes to shifting the largest counter ion accumulation zone (largest in the sense 'in line with the absence of NP charge reversal', see ref 1) closer to the particle surface (see argument detailed in ref 1 and Figure 5 therein). Effectively, the outcome is similar to that explained in the note 'NA[a]' upon increasing solution ionic strength.

There is no companion log $\overline{K}_{int}$ *vs.* log θ_M plot for the data in Table S2 because $\overline{f}_B^{(eq)}$ values could not be computed for all of the electrolyte conditions.

Table S3. Comparison of Computed and Experimentally-Derived Magnitudes of the Electrostatic Boltzmann Partitioning Coefficient, $\overline{f}_B$, for Divalent Cations for the case of r_p = 0.8 nm, charge density = -2184 mol *e* m^{-3}, and water content = 72%. Values in parentheses correspond to different spatial zones of counterion accumulation. Experimental data correspond to Cd(II) and Cu(II) binding by FA.

Electrolyte and ionic strength	**Theoretical**		**Experimental**
	equilibrated charge, $\overline{f}_B^{(eq)}$	structural charge, $\overline{f}_B^{(s)}$	Figure 3[d]
KNO_3, I = 10 mM	19.29 [b] (4.59 [a])	6.71 [a] (19.15 [b])	26 (12-57)
KNO_3, I = 100 mM	0.66 [b] (NA [a])	1.94 [a] (4.04 [b])	5 (3-10)
$Ca(NO_3)_2$, I = 10 mM	6.45 [n_{Ca}=1.19] [a] (27.73 [n_{Ca}=1.36] [b]) (3.37 [n_{Ca}=1.02] [c])	3.89 [a] (9.53 [b])	5 (3-10)
$Ca(NO_3)_2$, I = 100 mM	0.79 [b] (NA [a])	1.53 [a] (2.66 [b])	1[e]

[a] integral from r = 0 to $r = r_p$ + 2 nm

[b] integral from r = 0 to $r = r_p$ + 1 nm

[c] integral from r = 0 to $r = r_p$ + 2.5 nm

[d] experimental $\overline{f}_B$ values are obtained from the difference between the dashed lines shown in Figure 3 in the main text. The range of values in parentheses is obtained from the standard errors on the regression lines (see Figure 2 caption in main text)

[e] reference electrolyte with *a priori* $\overline{f}_B$ value of unity

n_{Ca} is the average number of Ca^{2+} per FA

NA[a]: not applicable, because a 2 nm extension of the condensation volume from the FA surface significantly exceeds the 0.96 nm extraparticulate Debye length operational in 100 mM solution ionic strength

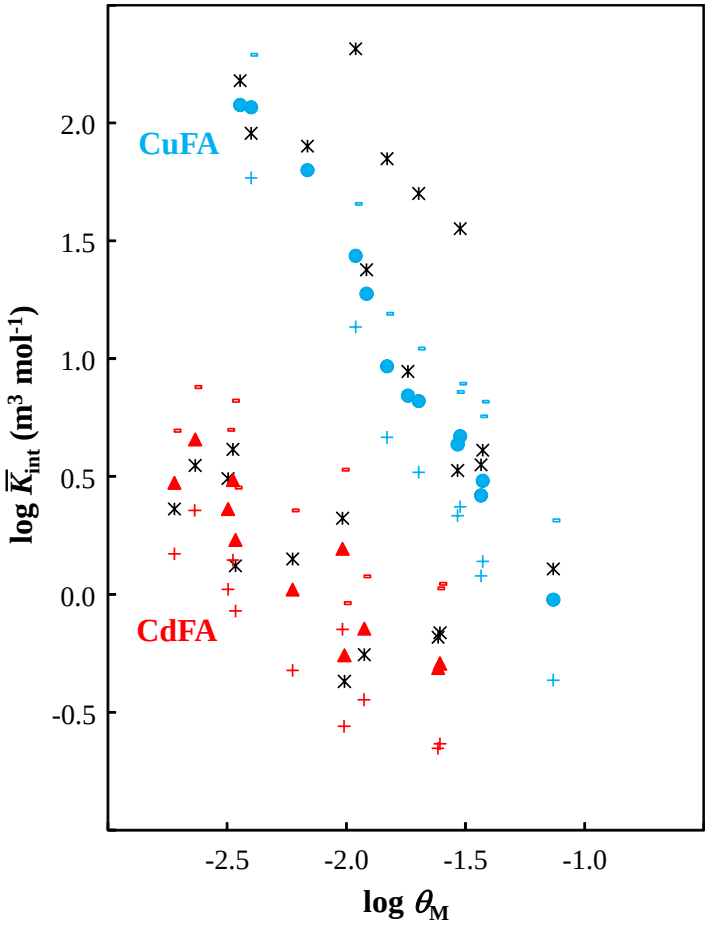

Figure S4. Comparison of the intrinsic stability constants, $\overline{K}_{int}$, determined for Cd(II) and Cu(II) complexes with fulvic acid (FA) as a function of the degree of occupation of reactive sites by inner-sphere complexes, i.e. the true θ_M (eq 7, main text). The relevant FA parameters are r_p = 0.8 nm, charge density = -2184 mol *e* m^{-3} and water content = 72%. The solid coloured points for CdFA (red triangles) and CuFA (blue dots) are obtained using the experimentally derived $\overline{f}_B$ values (Table 1, main text). The "+ "and "-" symbols correspond to the upper and lower limits of the experimentally derived $\overline{f}_B$ values. The black asterisks are the values obtained using the modelled $\overline{f}_B^{(eq)}$ values (Table S3, values not in parentheses). The RMSE between the modelled and experimental $\overline{K}_{int}$ values = 0.375.

Table S4. Comparison of Computed and Experimentally-Derived Magnitudes of the Electrostatic Boltzmann Partitioning Coefficient, $\overline{f}_B$, for Divalent Cations for the case of r_p = 0.8 nm, charge density = -4212 mol *e* m^{-3}, and water content = 46%. Values in parentheses correspond to different spatial zones of counterion accumulation. Experimental data correspond to Cd(II) and Cu(II) binding by FA.

Electrolyte and ionic strength	Theoretical		Experimental
	equilibrated charge, $\overline{f}_B^{(eq)}$	structural charge, $\overline{f}_B^{(s)}$	Figure 3[d]
KNO_3, I = 10 mM	38.25 [b] (10.09 [a])	120.58 [a] (443.28 [b])	26 (12-57)
KNO_3, I = 100 mM	4.02 [b] (NA [a])	6.17 [a] (19.63 [b])	5 (3-10)
$Ca(NO_3)_2$, I = 10 mM	13.56 [n_{Ca}=2.51] [a] (54.48 [n_{Ca}=2.68] [b]) (7.71 [n_{Ca}=2.33] [c])	9.46 [a] (29.29 [b])	5 (3-10)
$Ca(NO_3)_2$, I = 100 mM	3.48 [b] (NA [a])	2.16 [a] (4.89 [b])	1[e]

[a] integral from r = 0 to $r = r_p$ + 2 nm

[b] integral from r = 0 to $r = r_p$ + 1 nm

[c] integral from r = 0 to $r = r_p$ + 2.5 nm

[d] experimental $\overline{f}_B$ values are obtained from the difference between the dashed lines shown in Figure 3 in the main text. The range of values in parentheses is obtained from the standard errors on the regression lines (see Figure 2 caption in main text)

[e] reference electrolyte with *a priori* $\overline{f}_B$ value of unity

n_{Ca} is the average number of Ca^{2+} per FA

NA[a]: not applicable, because a 2 nm extension of the condensation volume from the FA surface significantly exceeds the 0.96 nm extraparticulate Debye length operational in 100 mM solution ionic strength

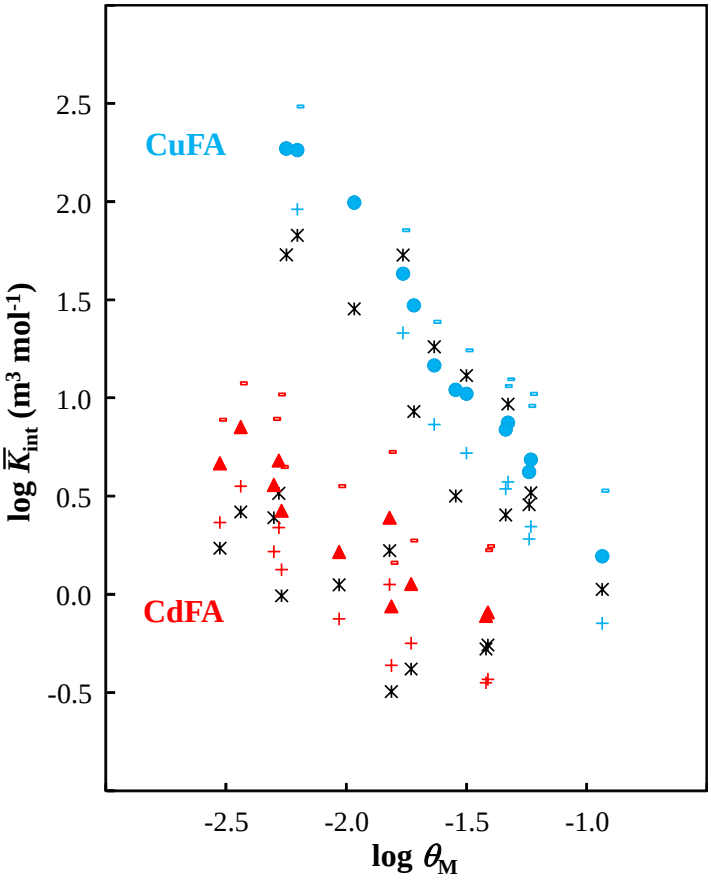

Figure S5. Comparison of the intrinsic stability constants, $\overline{K}_{int}$, determined for Cd(II) and Cu(II) complexes with fulvic acid (FA) as a function of the degree of occupation of reactive sites by inner-sphere complexes, i.e. the true θ_M (eq 7, main text). The relevant FA parameters are r_p = 0.8 nm, charge density = -4212 mol *e* m^{-3} and water content = 46%. The solid coloured points for CdFA (red triangles) and CuFA (blue dots) are obtained using the experimentally derived $\overline{f}_B$ values (Table 1, main text). The "+ "and "-" symbols correspond to the upper and lower limits of the experimentally derived $\overline{f}_B$ values. The black asterisks are the values obtained using the modelled $\overline{f}_B^{(eq)}$ values (Table S4, values not in parentheses). The RMSE between the modelled and experimental $\overline{K}_{int}$ values = 0.340.

Table S5. Comparison of Computed and Experimentally-Derived Magnitudes of the Electrostatic Boltzmann Partitioning Coefficient, $\overline{f}_B$, for Divalent Cations for the case of r_p = 1.5 nm, charge density = -312 mol *e* m^{-3}, and water content = 96%. Values in parentheses correspond to different spatial zones of counterion accumulation. Experimental data correspond to Cd(II) and Cu(II) binding by FA.

Electrolyte and ionic strength	**Theoretical**		**Experimental**
	equilibrated charge, $\overline{f}_B^{(eq)}$	structural charge, $\overline{f}_B^{(s)}$	Figure 3[d]
KNO_3, I = 10 mM	6.25 [b] (1.54 [a])	2.42 [a] (3.85 [b])	26 (12-57)
KNO_3, I = 100 mM	NA[b] (NA [a])	1.28 [a] (1.65 [b])	5 (3-10)
$Ca(NO_3)_2$, I = 10 mM	2.38 [n_{Ca}=0.86] [a]	2.18 [a] (3.34 [b])	5 (3-10)
	(8.98 [n_{Ca}=1.18] [b])		
	(1.04 [n_{Ca}=0.56] [c])		
$Ca(NO_3)_2$, I = 100 mM	NA[b] (NA [a])	1.24 [a] (1.55 [b])	1[e]

[a] integral from r = 0 to $r = r_p$ + 2 nm

[b] integral from r = 0 to $r = r_p$ + 1 nm

[c] integral from r = 0 to $r = r_p$ + 2.5 nm

[d] experimental $\overline{f}_B$ values are obtained from the difference between the dashed lines shown in Figure 3 in the main text. The range of values in parentheses is obtained from the standard errors on the regression lines (see Figure 2 caption in main text)

[e] reference electrolyte with *a priori* $\overline{f}_B$ value of unity

n_{Ca} is the average number of Ca^{2+} per FA

NA[a]: not applicable, because a 2 nm extension of the condensation volume from the FA surface significantly exceeds the 0.96 nm extraparticulate Debye length operational in 100 mM solution ionic strength

NA[b]: not applicable. Indeed, decreasing the charge density (in absolute value) comes to shifting the largest counter ion accumulation zone (largest in the sense 'in line with the absence of NP charge reversal', see ref 1) closer to the particle surface (see argument detailed in ref 1 and Figure 5 therein). Effectively, the outcome is similar to that explained in the note 'NA[a]' upon increasing solution ionic strength.

There is no companion log $\overline{K}_{int}$ *vs.* log θ_M plot for the data in Table S5 because $\overline{f}_B^{(eq)}$ values could not be computed for all of the electrolyte conditions.

.

Table S6. Comparison of Computed and Experimentally-Derived Magnitudes of the Electrostatic Boltzmann Partitioning Coefficient, $\overline{f}_B$, for Divalent Cations for the case of r_p = 1.5 nm, charge density = -624 mol *e* m^{-3}, and water content = 92%. Values in parentheses correspond to different spatial zones of counterion accumulation. Experimental data correspond to Cd(II) and Cu(II) binding by FA.

Electrolyte and ionic strength	**Theoretical**		**Experimental**
	equilibrated charge, $\overline{f}_B^{(eq)}$	structural charge, $\overline{f}_B^{(s)}$	Figure 3[d]
KNO_3, I = 10 mM	13.74 [b] (4.57 [a])	7.97 [a] (17.55 [b])	26 (12-57)
KNO_3, I = 100 mM	NA[b] (NA [a])	1.80 [a] (2.93 [b])	5 (3-10)
$Ca(NO_3)_2$, I = 10 mM	6.07 [n_{Ca}=2.19] [a] (19.10 [n_{Ca}=2.51] [b]) (3.51 [n_{Ca}=1.89] [c])	4.36 [a] (8.52 [b])	5 (3-10)
$Ca(NO_3)_2$, I = 100 mM	NA[b] (NA [a])	1.53 [a] (2.25 [b])	1[e]

[a] integral from r = 0 to $r = r_p$ + 2 nm

[b] integral from r = 0 to $r = r_p$ + 1 nm

[c] integral from r = 0 to $r = r_p$ + 2.5 nm

[d] experimental $\overline{f}_B$ values are obtained from the difference between the dashed lines shown in Figure 3 in the main text. The range of values in parentheses is obtained from the standard errors on the regression lines (see Figure 2 caption in main text)

[e] reference electrolyte with *a priori* $\overline{f}_B$ value of unity

n_{Ca} is the average number of Ca^{2+} per FA

NA[a]: not applicable, because a 2 nm extension of the condensation volume from the FA surface significantly exceeds the 0.96 nm extraparticulate Debye length operational in 100 mM solution ionic strength

NA[b]: not applicable. Indeed, decreasing the charge density (in absolute value) comes to shifting the largest counter ion accumulation zone (largest in the sense 'in line with the absence of NP charge reversal', see ref 1) closer to the particle surface (see argument detailed in ref 1 and Figure 5 therein). Effectively, the outcome is similar to that explained in the note 'NA[a]' upon increasing solution ionic strength.

There is no companion log $\overline{K}_{int}$ *vs.* log θ_M plot for the data in Table S6 because $\overline{f}_B^{(eq)}$ values could not be computed for all of the electrolyte conditions.

SSCP waves for CuHA

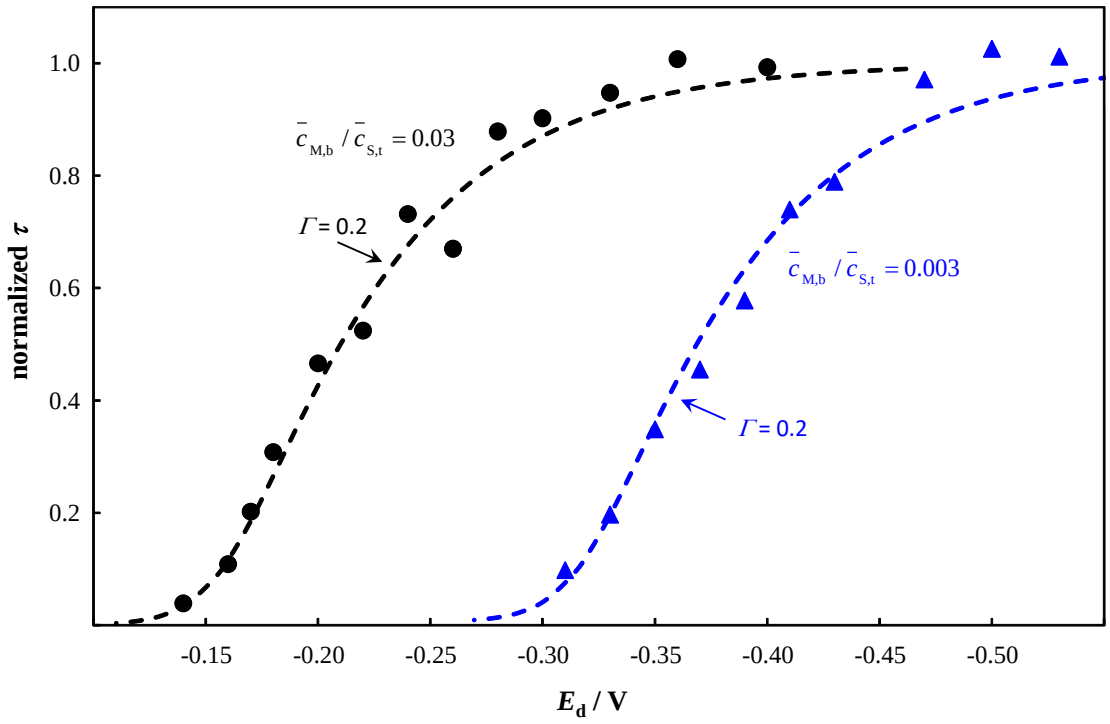

Figure S6. Experimental and computed SSCP waves (normalized reoxidation time, τ, as a function of deposition potential, E_d) for Cu(II) complexes with humic acid at pH 6 in $Ca(NO_3)_2$ electrolyte at I = 100 mM. Points are experimental data; dashed curves are computed for the Γ values indicated on the figure.

REFERENCES

(1) Duval, J. F. L.; Town, R. M.; van Leeuwen, H. P. Poisson-Boltzmann electrostatics and ionic partition equilibration of charged nanoparticles in aqueous media. *J. Phys. Chem C.* **2018**, *122*, 17328-17337.

(2) Duval, J. F. L.; Ohshima, H. Electrophoresis of diffuse soft particles. *Langmuir* **2006**, *22*, 3533-3546.

(3) Ohshima, H. Donnan potential and surface potential of a spherical soft particle in an electrolyte solution. *J. Coll. Interf. Sci.* **2008**, *323*, 92-97.

(4) Ohshima, H.; Kondo, T. Relationship among the surface potential, Donnan potential and charge density of ion-penetrable membranes. *Biophys. Chem.* **1990**, *38*, 117-122.

(5) Dinar, E.; Mentel, T. F.; Rudich, Y. The density of humic acids and humic like substances (HULIS) from fresh and aged wood burning and pollution aerosol particles. *Atmos. Chem. Phys.* **2006**, *6*, 5213-5224.

(6) Aiken, G. R.; Malcolm, R. L. Molecular weight of aquatic fulvic acids by vapor pressure osmometry. *Geochim. Cosmochim. Acta* **1987**, *51*, 2177-2184.

(7) Rostad, C. E.; Leenheer, J. A. 2004. Factors that affect molecular weight distribution of Suwannee river fulvic acid as determined by electrospray ionization/mass spectrometry. *Anal. Chim. Acta* **2004**, *523*, 269-278.

(8) Guéguen, C.; Cuss, C. W. Characterization of aquatic dissolved organic matter by asymmetrical flow field-flow fractionation coupled to UV-Visible diode array and excitation emission matrix fluorescence. *J. Chromatogr. A* **2011**, *1218*, 4188-4198.

(9) Lead, J. R.; Wilkinson, K. J.; Balnois, E.; Cutak, B. J.; Larive, C. K.; Assemi, S.; Beckett, R. Diffusion coefficients and polydispersities of the Suwannee River fulvic acid: comparison of fluorescence correlation spectroscopy, pulsed-field gradient nuclear magnetic resonance, and flow field-flow fractionation. *Environ. Sci. Technol.* **2000**, *34*, 3508-3513.

(10) Ritchie, J. D.; Perdue, E. M. Proton-binding study of standard and reference fulvic acids, humic acids, and natural organic matter. *Geochim. Cosmochim. Acta*, **2003**, *67*, 85-96.